Journal of Thermal Analysis, Vol. 53 (1998) 769-784

THE Al–Zn–Ga PHASE DIAGRAM
Part I

E. Aragon, K. Jardet, P. Satre and A. Sebaoun

Laboratoire de Physico-Chimie du Matériau et du Milieu Marin, Matériaux à Finalité Spécifique (E.A. 1356), Université de Toulon et du Var, B.P. 132, 83957 La Garde cedex, France

(Received August 8, 1997)

Abstract

The Al–Zn–Ga ternary phase diagram was earlier established by thermodynamic modellization [1], but no experimental study appears to have been carried out on this system, except for measurements of mixing enthalpies in the liquid [2].

The present experimental study was carried out by thermal analysis and X-ray diffraction at various temperatures, using the isopletic cuts method.

Four isopletic cuts were established and two others were partly studied in the Al-rich corner of the diagram. On these cuts, two isobaric ternary invariant reactions were determined: a eutectic reaction at 23±1°C, and a metatectic reaction at 123±1°C. Evidence was found for the existence of a retrograde miscibility of Ga in a solid solution α_{ss}' which protrudes into the ternary system starting from the Al–Zn binary up to a Ga concentration of about 30%*.

Keywords: Al–Zn–Ga ternary system, phase diagram, retrograde miscibility, thermal analysis, X-ray diffraction at various temperatures

Introduction

The Al–Zn binary phase diagram [3] (Fig. 1a) is a eutectic system involving a monotectoid reaction and a miscibility gap in the solid state. The Al solid solution has an extended homogeneity range, interrupted at lower temperatures by the miscibility gap. This solid solution is labelled α_{ss} on the Al-rich side (α_{ss} is a fcc (A1) solid solution) and α_{ss}' on the Zn-rich side (α_{ss}' has a rhombohedral structure [3] which corresponds to the α_{ss} structure, where one of the ternary axes has been slightly stretched).

The Al–Ga [4] (Fig. 1b) and Ga–Zn [4] (Fig. 1c) binary phase diagrams are eutectic systems. The solubilities, in the solid state, of Ga in Zn and of Zn in Ga

* Compositions are all given as mass percentages.

1418–2874/98/ $ 5.00

Akadémiai Kiadó, Budapest
Kluwer Academic Publshers, Dordecht

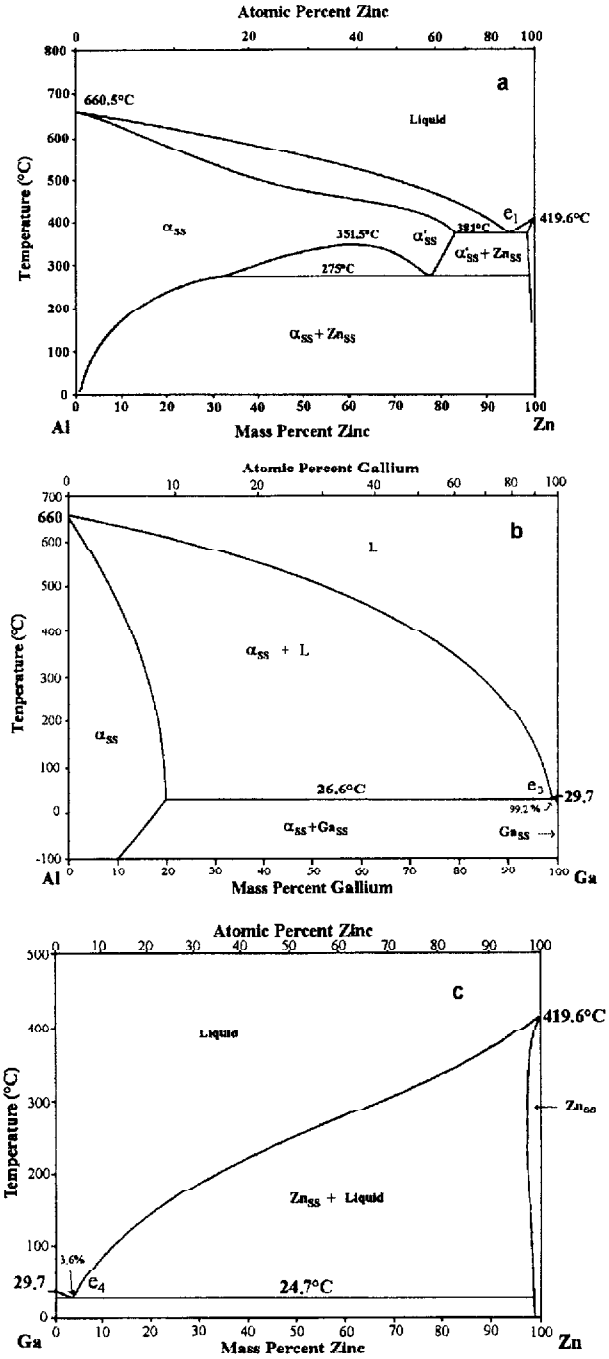

Fig. 1 Binary phase diagrams. a – Al–Zn binary phase diagram from [3], b – Al–Ga binary phase diagram from [4], c – Ga–Zn binary phase diagram from [4]

are very low. Al also has a very limited solubility in Ga, but the solubility of Ga in Al is 20%.

The Al–Ga, Al–Zn and Ga–Zn binary phase diagrams are well known, but the Al–Zn–Ga ternary phase diagram has never been subject to experimental study, although a thermodynamic computer version of this diagram has been published [1]. In that version, a ternary eutectic in the Ga-rich corner was calculated at 22°C:

$$L_E \leftrightarrows Zn_{ss} + \alpha_{ss} + Ga_{ss} \quad \Delta H < 0$$

The calculated composition of the isobaric invariant liquid is 0.68% Al, 96% Ga, 3.32% Zn.
At 282°C, an invariant reaction occurs, which is a transitory peritectic:

$$L_P + \alpha'_{ss} \leftrightarrows Zn_{ss} + \alpha_{ss} \quad \Delta H < 0$$

The calculated composition of the isobaric invariant liquid is 6.76% Al, 33.96% Ga, 59.28% Zn.

The calculated isothermal sections [1] indicate that the ($L+\alpha_{ss}$) phase region coalesces in the ternary with the ($\alpha'_{ss}+\alpha_{ss}$) phase region which originates at 351.5°C (binary critical point) in the Al–Zn binary system [3]. The coalescence of the two two-phase regions occurs at a calculated temperature of about 346.5°C [1] with the formation of a ($L+\alpha'_{ss}+\alpha_{ss}$) phase region. At that temperature, the ternary solid–solid critical point is conjugated to a vanishing point in the liquidus area, from which a monovariant line reaches the peritectic liquid.

These results on the ternary system Al–Zn–Ga are very similar to those presented for the Al–Zn–Sn ternary phase diagram [5–8], but are different from the ternary diagrams for Al–Zn–Si [9] or Al–Zn–Ge [10].

An experimental determination of the Al–Zn–Ga phase diagram was necessary to confirm the results.

Experimental

This experimental study was carried out by means of thermal analysis and X-ray diffraction at various temperatures, using the isopletic cuts method. Four main isopletic cuts (Fig. 2) were chosen, using the data given by Ansara [1]: ZA7-Ga $\left(\frac{m_{Al}}{m_{Al}+m_{Zn}}=0.07\right)$, ZA15-Ga, ZA20-Ga and ZA40-Ga (Fig. 2). On these isopleths, the compositions and temperatures of the ternary invariant equilibria were determined. The miscibility fields in the solid state were also identified. In addition, two isopletic cuts were partly studied in order to determine the limits of the isobaric ternary invariants in the Al-rich corner: ZA74-AGa52 and ZA88-AGa22 (Fig. 2).

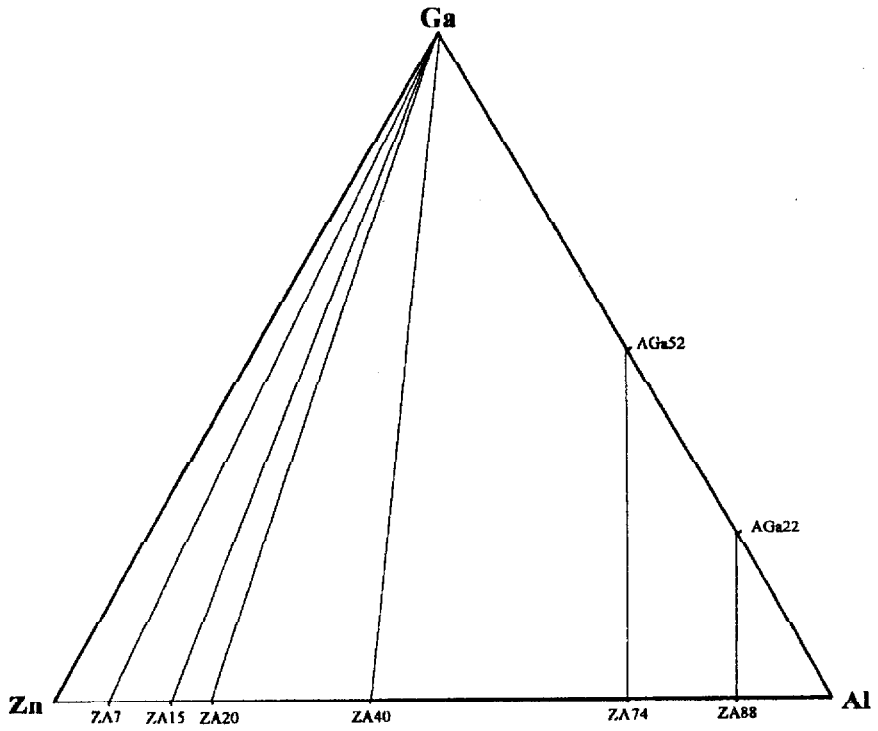

Fig. 2 Isopletic cuts for the experimental study

The samples were prepared by weighing and mixing pure Al, Zn and Ga (99.999%).

Differential thermal analysis (DTA) measurements were carried out with a TG/DTA 92-Setaram instrument to evaluate the possible mass loss associated with Zn vaporization. A Differential Scanning Calorimeter (DSC 92-Setaram) was also used: this allows invariant calorimetric measurements (Tammann method) and low-temperature investigations by cooling with liquid nitrogen. Stainless steel crucibles sealed with copper joins were used to prevent Zn vaporization and alloy oxidation. The temperature range used was from –50 to 550°C. The thermal analysis curves were recorded both on heating and on cooling. A heating and cooling rate of 5°C min^{-1} was used. The precision obtained after calibration was ±1°C for temperature measurements and about 10% for enthalpy determinations. Each composition studied on the different isopletic cuts was studied in three successive thermal cycles.

An X-ray diffraction powder method was used with $CuK_{\bar{\alpha}}$ radiation (λ= 0.15405 nm) at different temperatures ranging from room temperature up to 420°C. The Anton-Paar HTK10 high-temperature camera on the Philips PW 1050/20 goniometer was employed. The experiments were carried out under

inert gas (helium). The thermal sequences and the goniometer θ/2θ scanning were computer-assisted. A computer program also permitted X-ray diffraction data acquisition and treatment [11].

The samples were prepared by melting and dropping onto a cold sheet to obtain a thin homogeneous foil. The Pt heating rod was protected with a thin Mo foil (2.10–1 mm) from attack by liquid Ga-rich alloys. To take into account any preferred orientation of the crystallites, we compared the X-ray spectra of annealed foils with those of powders obtained by grinding at liquid nitrogen temperature.

To correct the thermal gradient between the upper side of the sample and the indication given by the thermocouple which controls the thermal regulation of the Pt heating rod and which indicates the sample temperature [12], we had to calibrate these temperatures in the range of study (25 to 450°C) by determining the melting points of high-purity In, Sn and Zn. This calibration needed very slow heating, with X-ray diffraction recording in steps of 1°C near the melting temperature and an annealing time of 15 min for each step. The maximum precision after this calibration for the present results is +1°C.

Preliminarily, a direction-finder calibration of the goniometer was carried out.

Data acquisition was preceded by an initial annealing time of 20 min for each step. Hence, the total annealing time (initial annealing plus θ-scanning time) was 50 min. To prevent metastable equilibria, some experiments were conducted with a long annealing time (more than 24 h). Several experiments were recorded for each sample and compared on heating and cooling.

The literature gives X-ray diffraction patterns for the high-purity metals Al [13], Zn [13] and Ga [14] at 25°C. The corresponding solid solutions at different temperatures were identified by extrapolation from these room temperature data. X-ray diffraction data are available on the binary α'_{ss} solid solution [15]. These authors worked on a quenched Al (29 at.%)-Zn binary alloy and identified a metastable transition phase with a trigonal deformed Al (fcc) structure. We observed similar spectra at different temperatures for a binary Al (38 at.%)-Zn alloy (in the α'_{ss} one-phase field between 275 and 400°C). These spectra were taken as references for identification of the α'_{ss} solid solution diffraction lines in the ternary alloys.

In any case, a comparison with reference data has to take into account the θ shift due to the thermal dilatation and the large solubility variation with temperature.

Results

The four isopletic cuts ZA7-Ga, ZA15-Ga, ZA20-Ga and ZA40-Ga are presented in Figs 3–6 and Tables 1–4. These Figures summarize the results obtained by thermal analysis (thermal accidents on heating and cooling, and invariant calorimetric measurements) and X-ray diffraction (phases identified for different alloys and at various temperatures).

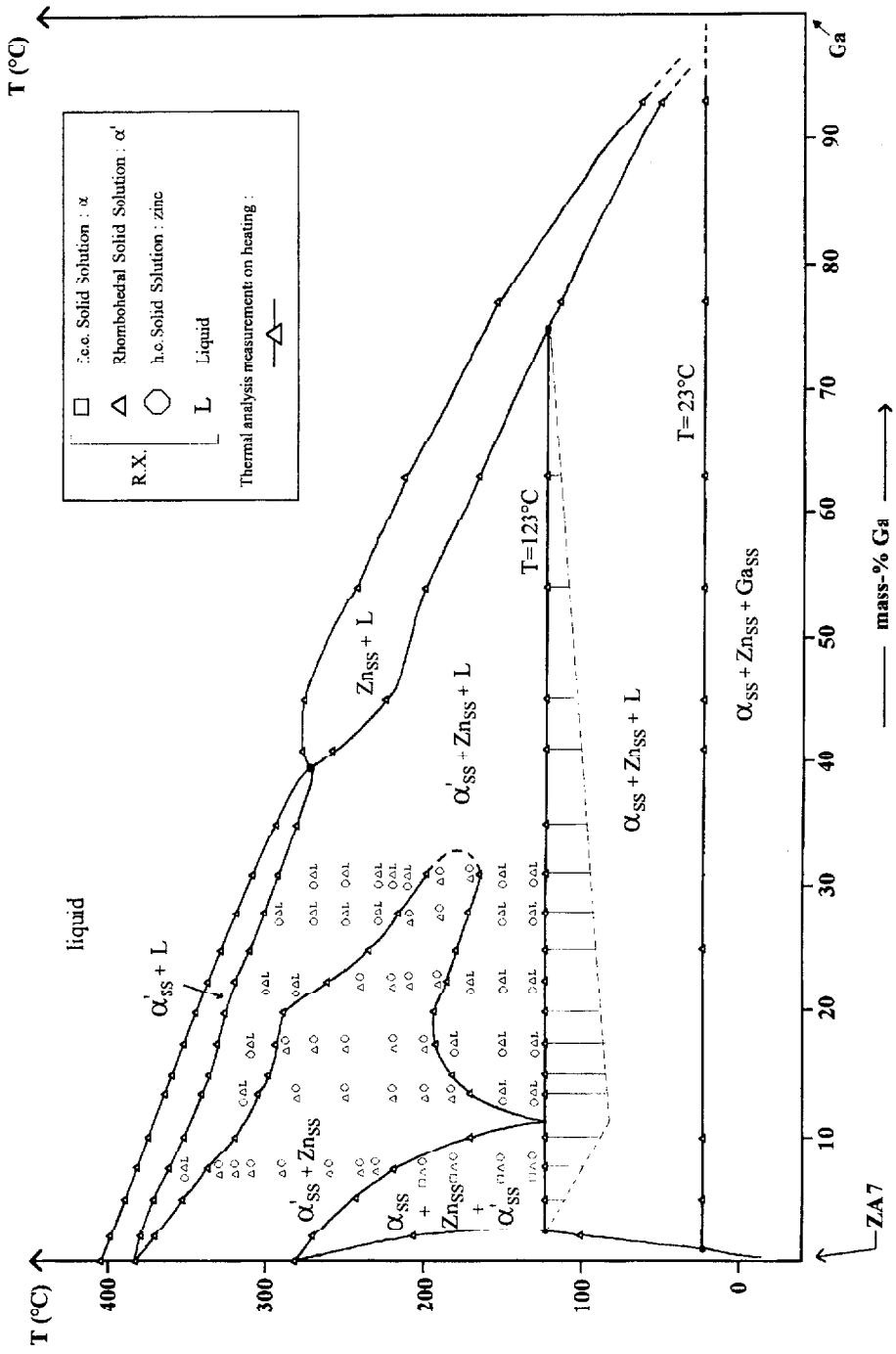

Fig. 3 ZA7-Ga isopletic cut

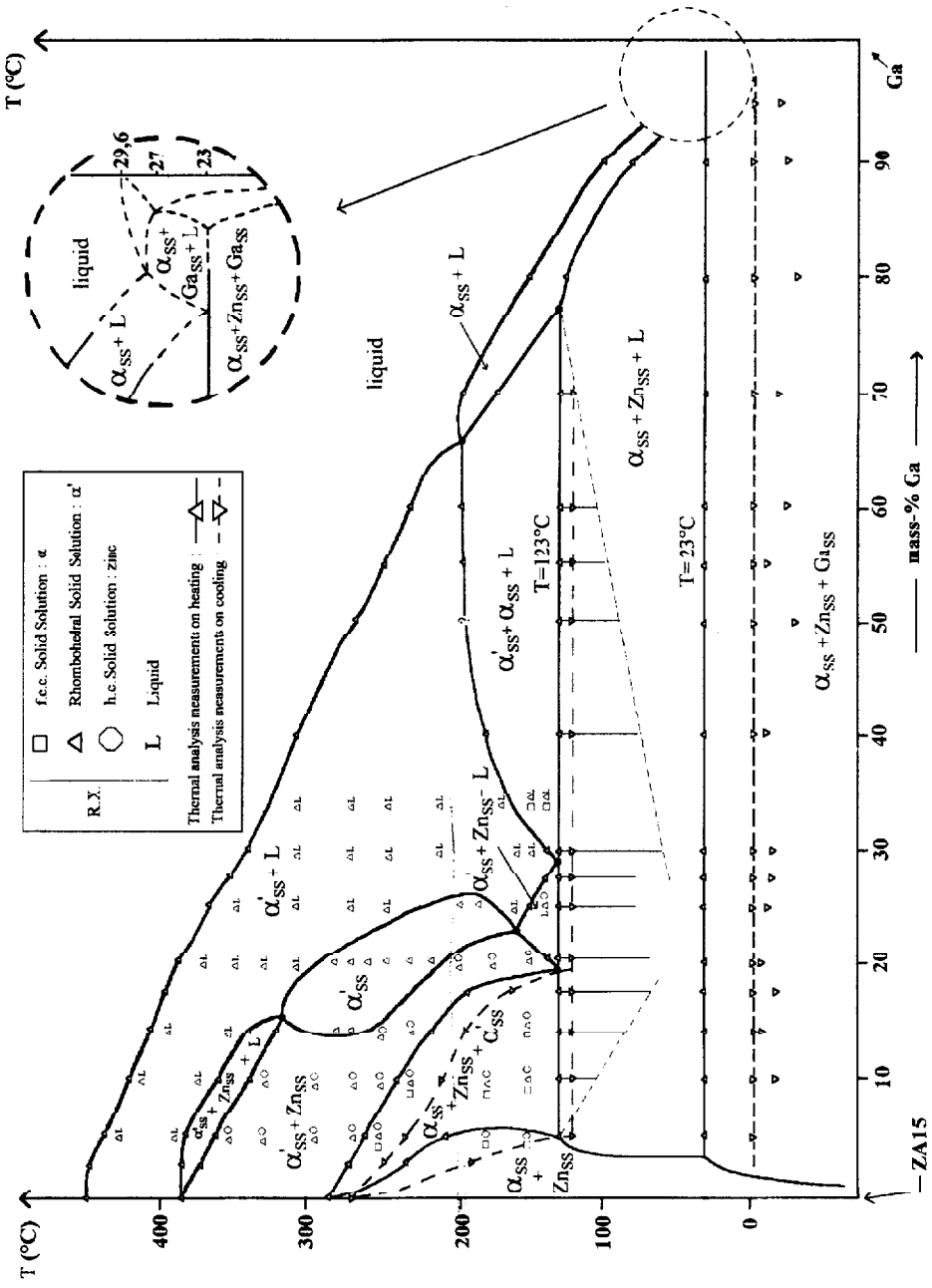

Fig. 4 ZA15-Ga isoplatic cut

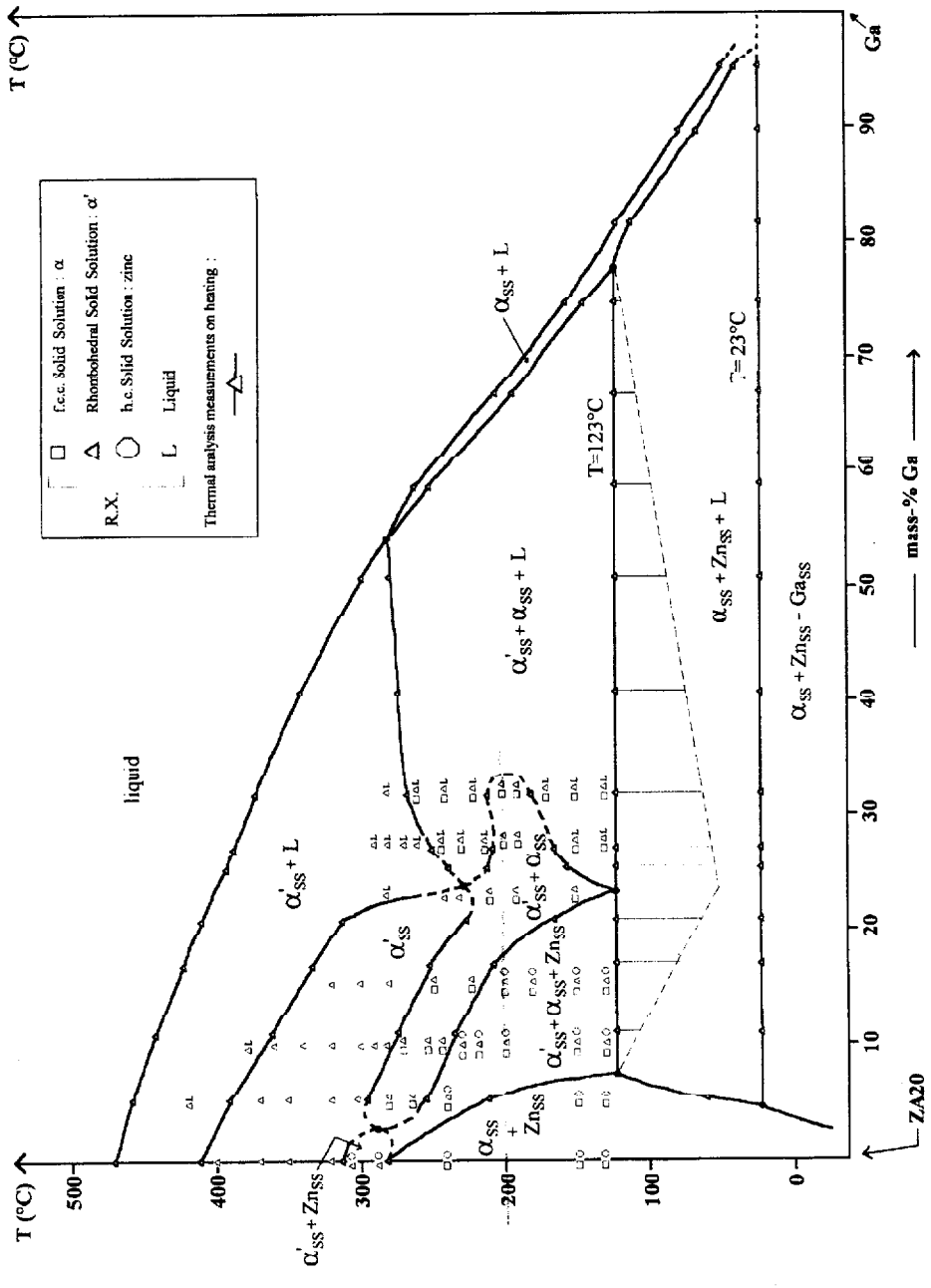

Fig. 5 ZA20-Ga isopleic cut

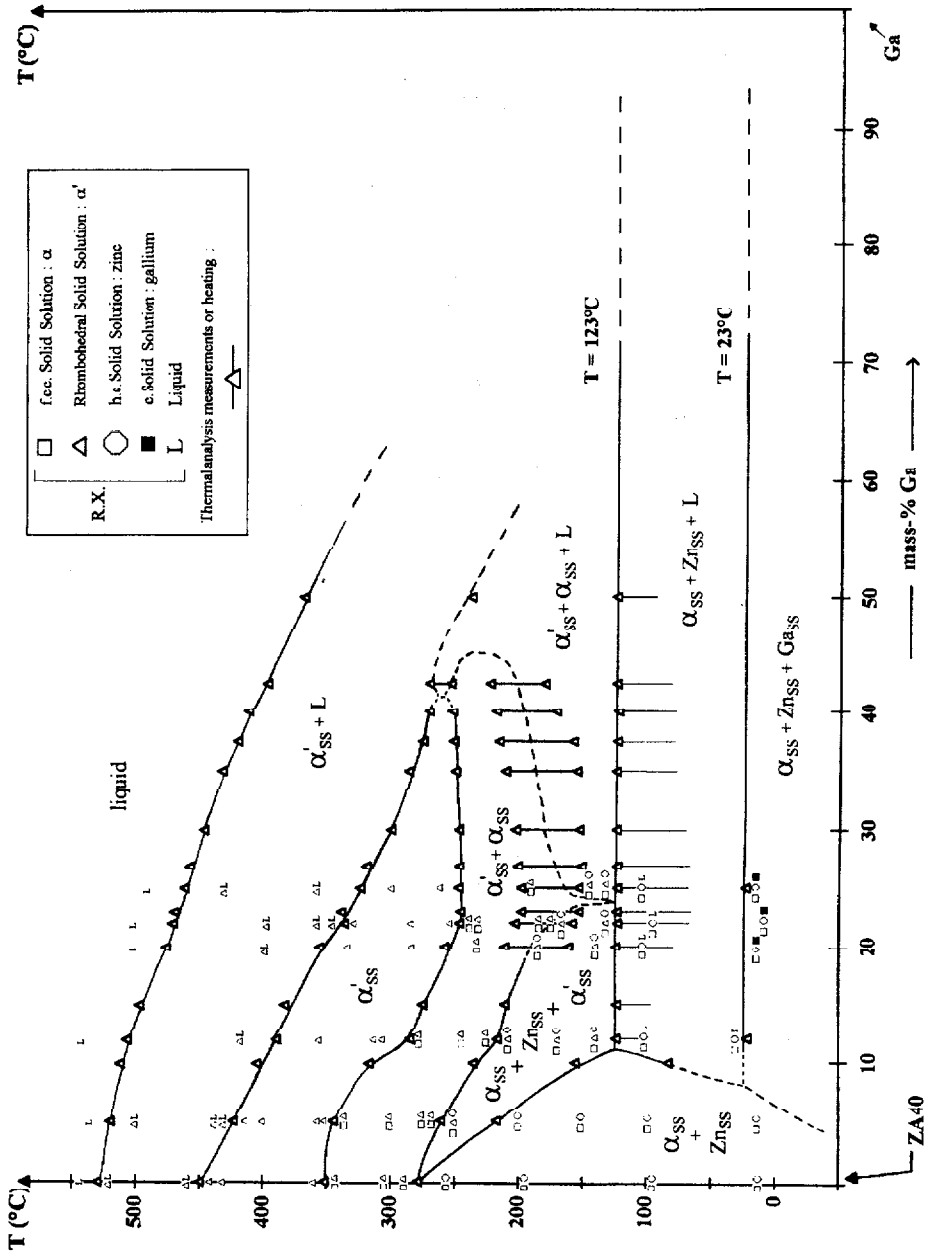

Fig. 6 ZA40-Ga isopletic cut

Table 1 Onset temperatures (°C) of thermal accidents on heating as a function of alloys composition on the ZA7-Ga isopletic cut

Mass percent of gallium on the isopletic cut ZA7-Ga	0	2	5	7.5	10	13.5	15	17.5	20	22.5	25	28	31	35	41	45	54	63	77	93
Fusion	403	398	388	376	367	356	350	343	335	330	320	315	306	297	277	276	242	213	155	61
Partial fusion: $SS_{\alpha}+SS_{Zn}+L \leftrightarrows SS_{\alpha'}+L$		379	370	360	351	340	335	331	326	320	309	305	296	283						
Partial fusion: $SS_{\alpha}+SS_{Zn}+L \leftrightarrows SS_{Zn}+L$															258	225	200	166		
(Binary eutectic Al–Zn)	383																			
$SS_{\alpha}+SS_{Zn} \leftrightarrows SS_{\alpha'}+SS_{Zn}+L$		370	352	336	319	305	298	294	288	260	234	215	198							
$SS_{\alpha}+SS_{Zn}+L \leftrightarrows SS_{\alpha'}+SS_{Zn}$						170	182	196	193	185	179	172	165							
(Binary monotectoid Al–Zn)	282																			
$SS_{\alpha}+SS_{Zn}+SS_{\alpha} \leftrightarrows SS_{\alpha'}+SS_{Zn}$		270	242	218	170															
$SS_{\alpha}+SS_{Zn} \leftrightarrows SS_{\alpha'}+SS_{Zn}+SS_{\alpha}$		206																		
Metatectic transformation: $SS_{\alpha}+SS_{Zn}+L \leftrightarrows SS_{\alpha'}$			123	123	123	124	123	124	122	124	123	124	124	122	123	123	123	123		
Partial fusion: $SS_{\alpha}+SS_{Zn}+L \leftrightarrows SS_{\alpha'}+L$																			114	49
$SS_{\alpha}+SS_{Zn}+L \leftrightarrows SS_{\alpha'}+SS_{Zn}$		100																		
Eutectic transformation: $SS_{\alpha}+SS_{Ga}+SS_{Zn} \leftrightarrows L_E$			23	23	23	22	22	24	23	24	23	22	23	23	23	23	22	23	23	24

Table 2 Onset temperatures (°C) of thermal accidents on heating as a function of alloys composition on the ZA15-Ga isopletic cut

Mass percent of gallium on the isopletic cut ZA15-Ga	0	2.5	5	10	14.1	17.5	20	25	27.5	30	40	50	55	60	70	80	90	95
Fusion	450	444	431	420	401	395	385	363	349	336	307	265	244	233	192	145	95	33
Partial fusion: $SS_{\alpha'}+SS_{Zn}+L \leftrightarrows SS_{\alpha'}+L$		376	381	356	336			155	137									
(Binary eutectic Al–Zn)	383																	
Partial fusion: $SS_{Zr}+SS_{\alpha'} \leftrightarrows SS_{\alpha'}+SS_{Zn}+L$		368	358	335	316													
(Binary monotectoid Al–Zn)	282																	
$SS_{\alpha'}+SS_{Zn}+SS_{\alpha} \leftrightarrows SS_{\alpha'}+SS_{Zn}$		268	258	230	210	198												
$SS_{\alpha}-SS_{Zn} \leftrightarrows SS_{\alpha'}+SS_{Zn}+SS_{\alpha}$		231	196															
Partial fusion: $SS_{\alpha'}+SS_{\alpha}+L+ \leftrightarrows SS_{\alpha'}+L$										139	182	?	198	201				
Partial fusion: $SS_{\alpha'}+SS_{\alpha}+L \leftrightarrows SS_{\chi}+L$															182			
$SS_{\alpha'}+SS_{Zn}+L \leftrightarrows SS_{\alpha'}+L$								154	138									
$SS_{\alpha'}+SS_{Zn}+L \leftrightarrows SS_{\alpha'}+SS_{Zr}$							135											
Metatectic transformation: $SS_{\alpha}+SS_{Zn}+L \leftrightarrows SS_{\alpha'}$			123	123	122	123	124	124	122	123	123	124	122	123	123			
Eutectic transformation: $SS_{\alpha}+SS_{Ga}+SS_{Zn} \leftrightarrows L_E$			23	22	22	24	23	23	23	24	22	23	23	24	23	24	23	23

Table 3 Onset temperatures (°C) of thermal accidents on heating as a function of alloys composition on the ZA20-Ga isopletic cut

Mass percent of gallium on the isopletic cut ZA20-Ga	0	5.3	11	17	21	25.5	27.3	32	41	51	59	67	75	82	90	95.5
Fusion	471	458	442	422	410	392	387	372	340	297	259	203	154	118	74	45
Partial fusion: $SS_{\alpha'} \leftrightarrows SS_{\alpha'} + L$	412	393	360	332	312											
Partial fusion: $SS_{\alpha} + SS_{\alpha'} + L \leftrightarrows SS_{\alpha'} + L$						238	250	266	272	278						
Partial fusion: $SS_{\alpha} + SS_{\alpha'} + L \leftrightarrows SS_{\alpha'} + L$											250	192	142			
$SS_{\alpha'} + SS_{Zn} \leftrightarrows SS_{\alpha'}$	314	296	274	252	225											
$SS_{\alpha'} + SS_{\alpha} \leftrightarrows SS_{\alpha} + SS_{\alpha'} + L$						211	207	211								
$SS_{\alpha'} + SS_{\alpha} + L \leftrightarrows SS_{\alpha} + SS_{\alpha'}$						156	165	181								
(Binary monotectoid Al–Zn)	282															
$SS_{\alpha'} + SS_{Zn} + SS_{\alpha} \leftrightarrows SS_{\alpha'} + SS_{\alpha}$		254	235	207	165											
$SS_{\alpha} + SS_{Zn} \leftrightarrows SS_{\alpha'} + SS_{Zn} + SS_{\alpha}$		212														
Metatectic transformation: $SS_{\alpha} + SS_{Zn} + L \leftrightarrows SS_{\alpha'}$			122	123	123	124	122	123	123	123	124	122	123			
Partial fusion: $SS_{\alpha} + SS_{Zn} + L \leftrightarrows SS_{\alpha} + L$														109	62	36
$SS_{\alpha} + SS_{Zn} + L \leftrightarrows SS_{\alpha} + SS_{Zn}$		60														
Eutectic transformation: $SS_{\alpha} + SS_{Ga} + SS_{Zn} \leftrightarrows L_E$			23	22	22	24	23	23	23	24	22	23	23	24	23	24

Table 4 Onset temperatures (°C) of thermal accidents on heating as a function of alloys composition on the ZA40-Ga isopletic cut

Mass percent of gallium on the isopletic cut ZA40-Ga	0	5	10	12	15	20	22	23	25	27	30	35	37.5	40	42.5	50
Fusion	530	520	512	507	497	476	471	469	461	458	446	433	420	412	397	368
Partial fusion: $SS_{\alpha'} \leftrightarrows SS_{\alpha} + L$	450	424	405	389	383	355	336	338	323	319	299	286	275			
Partial fusion: $SS_{\alpha} + SS_{\alpha'} + L \leftrightarrows SS_{\alpha'} + L$														270		237
(Binary demixtion Al–Zn)	352															
$SS_{\alpha'} - SS_{\alpha} \leftrightarrows SS_{\alpha'}$		345	317	285	275	257	246	245	246	246		250	251	252		
$SS_{\alpha'} - SS_{\alpha} \leftrightarrows SS_{\alpha} + SS_{\alpha'} + L$															253	
$SS_{\alpha'} + SS_{\alpha} + L \leftrightarrows SS_{\alpha} + SS_{\alpha'}$							157/ 202	152/ 197	152/ 197	150/ 200	152/ 202	154/ 210	157/ 215	170/ 217	179/ 222	
(Binary monotectoid Al–Zn)	279															
$SS_{\alpha'} + SS_{Zn} + SS_{\alpha} \leftrightarrows SS_{\alpha'} + SS_{\alpha}$		261	235	216	210	160/ 210										
$SS_{\alpha} + SS_{Zn} \leftrightarrows SS_{\alpha'} + SS_{Zn} + SS_{\alpha}$		217	155													
Metatectic transformation: $SS_{\alpha} + SS_{Zn} + L \leftrightarrows SS_{\alpha'}$				123	122	123	122	122	122	122	123	123	122	121	123	123
Partial fusion: $SS_{\alpha} + SS_{Zn} + L \leftrightarrows SS_{\alpha} + SS_{Zn}$			83													
Eutectic transformation: $SS_{\alpha} + SS_{Ga} + SS_{Zn} \leftrightarrows L_E$				21					22							

Two isobaric invariant reactions were observed:

– a ternary eutectic at 23±1°C on heating:

$$Zn_{ee} + \alpha_{ee} + Ga_{ee} \leftrightarrows L_E \quad \Delta H > 0$$

– and a ternary metatectic at 123±1°C on heating:

$$Zn_{ss} + \alpha_{ss} + L_M \leftrightarrows \alpha'_{ss} \quad \Delta H > 0$$

On cooling, the boundaries of the three-phase region ($Zn_{ss}+\alpha_{ss}+\alpha'_{ss}$) and the eutectic transformation were displaced toward lower temperatures. The metatectic reaction was measured at 109±1°C (Fig. 4). The eutectic transformation was displaced from 23°C on heating to –3°C on cooling. Thermal accidents were observed up to –30°C on cooling, depending on the composition (Fig. 4). These accidents seemed to correspond to the crystallization of two allotropic forms of Ga which are metastable at atmospheric pressure [16–18]. As a consequence, a liquid phase appeared at 23°C on heating and remained present on cooling to –30°C for some alloys.

On the ZA7-Ga isopletic cut (Fig. 3), X-ray diffraction at various temperatures [19, 20] revealed the existence of a solid two-phase field ($Zn_{ss}+\alpha'_{ss}$) which protruded into the three-phase field ($Zn_{ss}+\alpha'_{ss}+L$) up to a Ga concentration of about 30% [19, 20]. A solid two-phase field ($\alpha_{ss}+\alpha'_{ss}$), protruding into the three-phase field ($\alpha_{ss}+\alpha'_{ss}+L$), was also observed on the ZA20-Ga isopleth (Fig. 5) up to the same Ga concentration. Moreover, this isopleth exhibited a (α'_{ss}) one-phase field which protruded from the Al–Zn binary up to 20% of Ga. Crystallization of a Ga-rich liquid phase, with simultaneous solubilization of Ga in the α'_{ss} solid solution, was therefore observed on heating on the two isopletic cuts ZA7-Ga and ZA20-Ga.

This (α'_{ss}) one-phase field was also observed on the ZA15-Ga isopleth (Fig. 4). It was a closed field which did not reach the Al–Zn binary diagram on this isopleth. Thus, the (α'_{ss}) one-phase region flanked by the ($\alpha_{ss}+\alpha'_{ss}$) and ($Zn_{ss}+\alpha'_{ss}$) two-phase fields protruded into the ternary phase diagram from the Al–Zn binary diagram and extended in the direction of a high concentration of Ga.

As a consequence, the α'_{ss} ternary solid solution presents an important retrograde miscibility toward Ga.

Similar behaviour has been observed for Sn in the Al–Zn–Sn ternary phase diagram [5–8]. The similarity of the two diagrams might be due to interferences between the solid–solid and the liquid–solid equilibria because of the displacement of the liquidus area towards lower temperatures. The melting temperatures of Sn (T_M(Sn)=232°C) and Ga (T_M(Ga)=29°C), which are lower than those of Al (T_M(Al)=660°C) and Zn (T_M(Zn)=420°C), would explain this behaviour. In con-

trast, the phenomena observed in the Al–Zn–Sn ternary diagram [5–8] does not occur in the studied Al–Zn–Si [9] (T_M(Si)=1410°C) or Al–Zn–Ge [10] (T_M(Ge)=958°C) ternary diagrams.

Conclusions

The whole liquid–solid and solid–solid equilibria were studied experimentally by the isopletic cuts method. Two isobaric invariant reactions were observed by means of thermal analysis on heating: a eutectic at 23±1°C, which is in good agreement with that determined by modellization at 22°C [1], and a metatectic at 123±1°C, which does not agree with the calculated peritectic invariant at 282°C [1]. On cooling, the invariant transformation are displaced towards lower temperatures: the eutectic transformation is displaced to –3°C, but a liquid phase remains present to –30°C for some alloys. The existence of a liquid phase in these alloys at room temperature creates difficulties for metallographic studies and SEM investigations. The alloy ageing due to the presence of a liquid phase at room temperature is also a problem: the alloys must be cooled at liquid nitrogen temperature and preserved below 23°C. The existence or not of the liquid phase, depending on the thermal treatment, has a great influence on the elec trochemical behaviour of these alloys [21].

The results show the existence of a significant retrograde miscibility of Ga in the α'_{ss} solid solution which protrudes into the ternary system, starting from the Al–Zn binary up to a Ga concentration of about 30%. Similar behaviour has been observed for Sn in the Al–Zn–Sn ternary phase diagram [5–8].

* * *

The authors thank D.G.A./D.C.N. (Délégation Générale de l'Armement/Direction des Constructions Navales) of Toulon for financial support during preparation of the thesis by E. Aragon at Toulon University. In particular, the help of Mr. Giroud is gratefully acknowledged.

References

1 I. Ansara, G. Petzow and G. Effenberg ed., Ternary Alloys, 5 (1991) 552.
2 Bourkba, Thesis, Agadir University, Maroc, (1996).
3 J. L. Murray, Bulletin of Alloys Phase Diagrams, Vol. 4, 1 (1983) 55.
4 C. Girard, Thesis, Provence University, Marseille, France, (1985).
5 D. Vincent, Thesis, No. 81, Claude Bernard University, Lyon I, France, (1982).
6 D. Vincent and A. Sebaoun, J. Thermal Anal., 20 (1981) 419.
7 D. Vincent and A. Sebaoun, Mém. Etud. Sci. Rev. Métall., 78 (1981) 165.
8 A. Sebaoun, D. Vincent and D. Treheux, Materials Science and Technology, 3 (1987) 241.
9 C. Planchamp, Thesis, No. 33, Claude Bernard University, Lyon I, France, (1974).
10 E. Tadjbakhche, Thesis, Claude Bernard University, Lyon I, France, (1977).
11 B. Ducourant, R. Fourcade and G. Maschcrpa, Licence C.N.R.S./A.N.V.A.R., marketed by Philips.
12 N. E. Brown, S. M. Swapp, C. L. Bennet and A. Navrotsky, J. Appl. Cryst., 26 (1993) 77.

13 Swanson and Tatge, Natl. Bur. Stand. (U.S.), Circ. 539, 1 (1953) 11.
14 Swanson and Fuyat, Natl. Bur. Stand. (U.S.), Circ. 539, 2 (1953) 9.
15 K. K. Rao, H. Herman and E. Parthé, Mater. Sci. Eng., 1 (1966) 162.
16 A. Defrain, I. Epelboin et M. Erny, C. R. de l'Académie des Sciences, 250 (1960) 2553.
17 A. Defrain, I. Epelboin, C. R. de l'Académie des Sciences, 249 (1959) 50.
18 P. W. Bridgman, Phys. Rev., 48 (1935) 893.
19 E. Aragon, Thesis, Toulon University, France, (1995).
20 E. Aragon, K. Jardet, P. Satre and A. Sebaoun, Thermodynamics of Alloys, 2 to 5 sept. 1996 Marseille, France.
21 E. Aragon, L. Cazenave-Vergez, A. Giroud and A. Sebaoun, British Corrosion Journal, 52 (1997) 121.